Component and State Separation in DMPC/DSPC Lipid Bilayers: A Monte Carlo Simulation Study

Ekaterina I. Michonova-Alexova and István P. Sugár
Departments of Biomathematical Sciences and Physiology/Biophysics, Mount Sinai School of Medicine at New York University, New York, New York 10029 USA

ABSTRACT In this paper a two-state, two-component, Ising-type model is used to simulate the lateral distribution of the components and gel/fluid state acyl chains in dimyristoylphosphatidylcholine/distearoylphosphatidylcholine (DMPC/DSPC) lipid bilayers. The same model has been successful in calculating the excess heat capacity curves, the fluorescence recovery after photobleaching (FRAP) threshold temperatures, the most frequent center-to-center distances between DSPC clusters, and the fractal dimensions of gel clusters (Sugar, I. P., T. E. Thompson, and R. L. Biltonen, 1999. *Biophys. J.* 76:2099–2110). Depending on the temperature and mole fraction the population of the cluster size is either homogeneous or inhomogeneous. In the inhomogeneous population the size of the largest cluster scales with the size of the system, while the rest of the clusters remain small with increasing system size. In a homogeneous population, however, every cluster remains small with increasing system size. For both compositional and fluid/gel state clusters, threshold temperatures—the so-called percolation threshold temperatures—are determined where change in the type of the population takes place. At a given mole fraction, the number of percolation threshold temperatures can be 0, 1, 2, or 3. By plotting these percolation threshold temperatures on the temperature/mole fraction plane, the diagrams of component and state separation of DMPC/DSPC bilayers are constructed. In agreement with the small-angle neutron scattering measurements, the component separation diagram shows nonrandom lateral distribution of the components not only in the gel-fluid mixed phase region, but also in the pure gel and pure fluid regions. A combined diagram of component and state separation is constructed to characterize the lateral distribution of lipid components and gel/fluid state acyl chains in DMPC/DSPC mixtures. While theoretical phase diagrams of two component mixtures can be constructed only in the case of first-order transitions, state and component separation diagrams can be constructed whether or not the system is involved in first-order transition. The effects of interchain interactions on the component and state separation diagrams are demonstrated on three different models. The influences of state and component separation on the in-plane and off-plane membrane reactions are discussed.

INTRODUCTION

Cell membranes are complex formations, composed of a variety of lipids and proteins. It has been demonstrated that the lipids are of significant importance for the membrane functions as they exhibit distinct static and dynamic structural organization on a small scale, which involves formation of lipid clusters (Tocanne, 1992; Bergelson et al., 1995; Hwang et al., 1998). Recently, lipid clusters have been studied intensively in both biological and model membranes (Welty and Glaser, 1994; Mouritsen and Jørgensen, 1997; Brown and London, 1998; Leidy et al., 2001; Muresan et al., 2001). Under physiological temperatures the gel and the fluid phases coexist, and lipid clusters composed of molecules in either gel or in fluid phase can be formed. Such gel clusters represent areas of the membrane where the lateral diffusion of molecules is restricted (Kapitza et al., 1984), and thus biologically important in-plane reactions cannot occur. In-plane reactions may take place, however, in the fluid clusters of the membrane. The equilibrium poise and rates of the in-plane reactions may be significantly affected by the connectedness and percolation properties of the gel and fluid clusters (Melo et al., 1992; Thompson et al., 1995). Besides the fluid and gel clusters, compositional clusters, composed of the same lipid component, play an important role in membrane surface reactions such as activity of enzymes and receptors bound to the membrane (Glaser et al., 1996; Yang and Glaser, 1996; Honger et al., 1996; Dibble et al., 1996), morphological changes at the cell surface (Welby et al., 1996; Scheiffele et al., 1999), and gene expression (Norris and Madsen, 1995). The membrane trafficking and sorting have also been suggested to be influenced by formation of compositional clusters (Verkade and Simons, 1997; Mukherjee et al., 1999). Cholesterol and lipid clusters, also called rafts, participate in distributing proteins to the cell surface and to other organelles and play a significant role in many signaling cascades (Simons and Toomre, 2000) and in the activation of immune responses (Langlet et al., 2000).

The structure-function relationships of biological membranes have been studied for decades on model membranes. Because phosphatidylcholines are most abundant in biological membranes, DMPC/DSPC is the most thoroughly investigated two-component lipid bilayer (Koynova and Caffrey, 1998). The thermodynamic parameters of DMPC/DSPC bilayers have been examined experimentally by a number of experimental methods including differential scanning calorimetry (DSC) (Mabrey and Sturtevant, 1976; Van Dijck et al., 1977; Koynova and Caffrey, 1998),

Submitted December 12, 2001, and accepted for publication May 14, 2002.
Address reprint requests to István P. Sugár, One Gustav Levy Place, New York, NY 10029. Tel.: 212-241-8110; Fax: 212-860-4630; E-mail: sugar@camelot.mssm.edu.

0006-3495/02/10/1820/14 $2.00

dilatometry (Wilkinson and Nagle, 1979), densitometry (Schmidt and Knoll, 1986), neutron scattering (Knoll et al., 1981, 1983), nuclear magnetic resonance (NMR) (Lu et al., 1995; Sankaram and Thompson, 1992), ESR (Sankaram et al., 1992), Raman spectorscopy (Mendelsohn and Maisano, 1978), and Fourier transformed infrared spectroscopy (Brumm et al., 1996). The structural characteristics of the fluid and gel coexistence region have been examined experimentally by using fluorescance recovery after photobleaching (FRAP) (Vaz et al., 1989; Schram et al., 1996), fluorescence spectroscopy (Piknova et al., 1996), and electron spin resonance (ESR) (Sankaram et al., 1992). Based on the above-mentioned studies, it is presently well known that DMPC and DSPC form nonideal mixtures, i.e., there is a broad gel-fluid coexistence region in the phase diagram of this system (Wilkinson and Nagle, 1979; Mabrey and Sturtevant, 1976). The minor phase forms small clusters in the continuum of the major phase (Von Dreele, 1978). For many years only indirect detection of these small fluid and gel clusters had been possible (Sankaram et al., 1992; Pedersen et al., 1996). By means of atomic force microscopy (AFM) Gliss et al. (1998) were able to detect small gel clusters in an equimolar mixture of DMPC/DSPC supported bilayer down to *10 nm*, which is the resolution of the technique (personal communication with Dr. Kay Yee Lee, University of Chicago). Clusters more than three orders of magnitudes larger were recently visualized by fluorescence microscopy (Bagatolli and Gratton, 2000a,b) in giant unilamellar vesicles of equimolar DMPC/DSPC mixture. Only one or a small number of these large clusters were observed and their size was comparable to the size of the vesicle. By using small-angle neutron scattering Knoll et al. (1981) observed component separation below the solidus line and from 0.3 to 0.7 DMPC-d_{54}/DSPC mole fraction, and concluded that the phase diagram of DMPC/DSPC mixtures is peritectic. Unexpectedly, nonrandom distribution of the components was measured above the liquidus line and below 331 K in equimolar perdeutero-dimyristoylphoshatidylcholine/distearoylphosphatidylcholine (DMPC-d_{54}/DSPC) mixture, which phenomenon was explained by critical demixing (Knoll et al., 1983).

DMPC/DSPC mixtures have been thoroughly investigated theoretically as well (Von Dreele, 1978; Ipsen and Mouritsen, 1988; Brumbaugh et al., 1990; Brumbaugh and Huang, 1992; Jan et al., 1984; Jørgensen et al., 1993; Priest, 1980; Sugar and Monticelli, 1985). Among all the theoretical methods applied, only Monte Carlo simulations can provide information about the equilibrium lateral distribution of the lipid molecules in the bilayer (Nielsen et al., 2000; Scott et al., 1998; Sugar et al., 2001). The fact that along with the measurable properties of the system, currently immeasurable properties can also be obtained from the simulations is the major advantage of the method. We emphasize the simplicity of these models exemplified by the gel-fluid transition of one-component lipid bilayers, where it is assumed that each hydrocarbon chain exists in either gel or fluid state, and only nearest-neighbor interactions between the chains need to be considered. These models are so-called minimal models, making assumptions that are physically plausible and absolutely necessary for the correct simulation of the gel-fluid transition. As a consequence, the number of model parameters is minimal and the parameters have explicit physical meaning. The unique feature of this approach is that experimental data are used to estimate the values of the parameters. For the sake of simplicity, none of the above-mentioned 2D membrane models gave a combined description of the pre and main transition, which would increase the number of assumptions and model parameters. It is important to note, however, that in the case of multilamellar vesicles this simplification may produce incorrect prediction of domain shapes, primarily at the onset of the gel-to-fluid transition. To date only one simple, one-dimensional lattice model exists for the combined description of pre and main transition in a one-component system (Heimburg, 2000). In the case of DMPC giant unilamellar vesicles (Evans and Kwok, 1982), DPPC single bilayers (Hui, 1976), and DMPC and DPPC extruded unilamellar vesicles (Jutila and Kinnunen, 1997, and personal communication with Dr. P. K. J. Kinnunen) there is strong experimental evidence of the lack of pretransition.

Monte Carlo methods have been used to simulate the lateral distribution of the components in the pure gel or fluid phase regions (Jan et al., 1984). Jørgensen et al. (1993) applied a 10-state model to simulate the phase properties and the lateral distribution of the components in the one-phase and the gel-fluid coexistence region of DMPC/DSPC mixtures. Risbo et al. (1995) have studied the type of the gel-fluid transition in the same model by using Monte Carlo simulation in the grand canonical ensemble. Risbo and his co-workers pointed out that the gel-fluid transition in the pure DMPC or DSPC system is a continuous transition, but a first-order phase transition can be induced when small amounts of another species are mixed in the pure system. Sugar et al. (1999) described DMPC/DSPC bilayers by a two-state, two-component model in canonical ensemble using a set of parameters derived from a limited amount of experimental data. The analysis of the bilayer energy distribution function revealed that the gel-fluid transition is a continuous transition through equilibrium states for DMPC, DSPC, and DMPC/DSPC mixtures; i.e., the system is above the critical point. The same model successfully predicted the excess heat capacity curves and the FRAP threshold temperatures at different mole fractions, the most frequent center-to-center distance between DSPC clusters at different temperatures, the fractal dimensions of the gel clusters, and the upper bound for the size of the small, nonpercolated gel clusters, in good agreement with the respective experimental data (Sugar and Biltonen, 2000; Michonova-Alexova and Sugar, 2001; Sugar et al., 2001). Recently, the geometrical properties of the gel and fluid clusters, such as cluster

perimeter, cluster size, number of arms along the cluster perimeter, and number and size of inner islands in a host cluster were characterized in an equimolar mixture of DMPC/DSPC (Sugar et al., 2001). While considerable amount of data have been collected on the gel and fluid clusters in DMPC/DSPC bilayers, our knowledge of the compositional clusters is very limited.

In this paper we use our thoroughly tested two-state model of DMPC/DSPC bilayer to generate the size distributions of DMPC and DSPC clusters at different temperatures and mole fractions. A condensed description of the model is given in the Methods section. In the Results section, size distributions of the compositional clusters are presented. In the Discussion the diagrams of component and state separation of DMPC/DSPC bilayer are constructed. Comparison is made between the measured SANS data and the calculated diagram of component separation. The effects of the interchain interactions on the component and state separation diagrams are investigated. The effects of state and component separation on the in-plane and off-plane membrane reactions, respectively, are discussed. A combined state and component separation diagram is constructed for the overall characterization of the lateral distribution of the components and gel/fluid chains in DMPC/DSPC mixtures.

METHODS

Model of DMPC/DSPC bilayers

The two-state Ising-type (Ising, 1925) model of DMPC/DSPC lipid bilayers used in this work has been described in detail elsewhere (Sugar et al., 1999; Sugar and Biltonen, 2000). In this section only a brief description of the model will be given. Assuming symmetry of the lipid bilayer, only a single monolayer is modeled as a triangular lattice of N points. All acyl chains of DMPC and DSPC in either gel (g) or in fluid (f) state are located at the lattice points of the triangular lattice. It was experimentally shown that the chains of the lipid molecules in the gel state are organized on a triangular lattice (Janiak et al., 1979; Hui et al., 1995). At the gel-to-fluid transition, the crystalline order is lost and the lipid chains become fluid-disordered, but the chains remain closely packed. The best lattice to model the position of these closely packed double-chain molecules is, again, the triangular lattice.

In our model a phospholipid molecule is represented by a pair of nearest-neighbor acyl chains, linked covalently to each other. The number of DMPC and DSPC molecules is $N_1/2$ and $N_2/2$, respectively, where $N_1 + N_2 = N$ is the total number of the lattice points. Every lattice configuration can be uniquely described by a square matrix **S** and a connection vector **c**, both composed of N elements. Each one of the **S** matrix elements can take values 1, 2, 3, or 4, corresponding to DMPC acyl chain in gel state, DSPC acyl chain in gel state, DMPC acyl chain in fluid state, and DSPC acyl chain in the fluid state, respectively. The ith element of the connection vector c_i defines the location of the acyl chain covalently attached to the acyl chain at the ith lattice point.

The energy function of the system is the sum of intrachain and interchain energy terms. The intrachain energy E_j^m of an acyl chain of component j in state m is assumed constant and independent of location and orientation of the rotational isomers. The number of possible locations and orientations of the rotational isomers is characterized by f_j^m, the degeneracy of the energy level of component j in state m. E_{jk}^{mn} is the interchain energy between component j in state m and component k in state n. Only nearest-neighbor interactions are considered between the acyl chains because they are short-range van der Waals interactions. Calculating the lattice energy periodic boundary conditions are applied to eliminate the effects of the lattice edges (Huang, 1963) and also to reduce the number of model parameters. When fitting the model to a limited number of calorimetric data, the strategy of consecutive parameter estimation was utilized to get a robust set of model parameters (see the Determination of Model Parameters section and Table 1 in Sugar et al., 1999). The analysis of the bilayer energy distribution function revealed that the gel-fluid transition is a continuous transition through equilibrium states for DMPC, DSPC, and DMPC/DSPC mixtures; i.e., the system is above a critical point.

Steps in the Monte Carlo simulations

The thermal fluctuations of DMPC/DSPC bilayers can be simulated by means of Monte Carlo methods. The steps of the simulation have been described in detail elsewhere (Sugar et al., 1999; Sugar and Biltonen, 2000). Each simulation starts from an either all-gel or all-fluid state with similarly oriented molecules. During the simulation, trial configurations are generated in three different ways: 1) by changing the state of a randomly selected acyl chain from gel to fluid or from fluid to gel; 2) by exchanging two randomly selected molecules of different lipid components; and 3) by changing the orientation of a pair of randomly selected nearest-neighbor molecules. Each trial configuration is accepted or rejected according to the Metropolis criterion (Metropolis et al., 1953). A series of such elementary steps drives the system to equilibrium, i.e., to the equilibrium distribution of the molecules. The chain of elementary steps can be divided into Monte Carlo cycles. During each Monte Carlo cycle, the system has the opportunity to realize all of its configurations at least once. In our simulations, each Monte Carlo cycle consists of $2N$ elementary steps of local state alterations, followed by N_1 (or N_2 if $N_2 > N_1$) exchange steps and $4N/3$ reorientation steps. At the end of each Monte Carlo cycle, the state of each acyl chain is altered from gel to fluid or from fluid to gel. This nonphysical trial state generation is used to accelerate the attainment of the equilibrium distribution (Sun and Sugar, 1997). To calculate the size distribution of either DMPC or DSPC clusters, the snapshot is analyzed at the end of each Monte Carlo cycle by using the cluster counting program of Binder and Stauffer (1987).

RESULTS

Most of the simulations are performed on a triangular lattice of size 40×40, at different temperatures and DMPC/DSPC mole fractions. At this lattice size and in the range of 0.2 to 0.8 DMPC/DSPC mole fraction, the finite size effects on excess heat capacity are negligibly small (Sugar and Biltonen, 2000). Each simulation starts with 6000 Monte Carlo cycles, resulting in equilibration of the system, followed by 120,000 additional Monte Carlo cycles, unless otherwise stated. After equilibration the snapshots are analyzed at the end of each Monte Carlo cycle and the data are collected to generate the size distributions of DMPC and DSPC clusters, or gel and fluid state clusters.

Size distributions of compositional clusters

The size distributions of the compositional clusters are either unimodal or bimodal. In Fig. 1, examples for unimoal and bimodal size distributions of DSPC clusters are shown

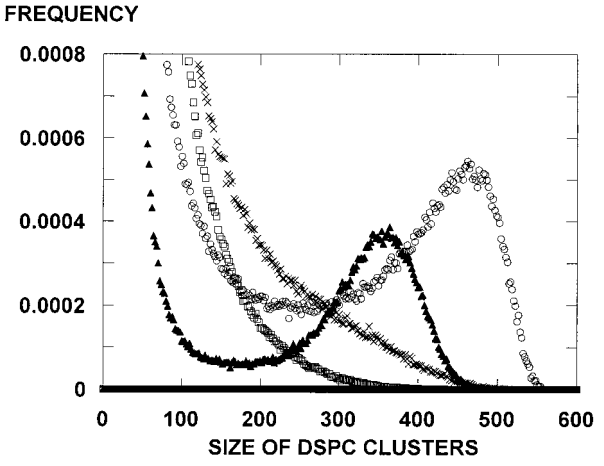

FIGURE 1 Size distributions of DSPC clusters in DMPC/DSPC (64:36) mixture. Bimodal distribution at $T = 220$ K (*open circles*); unimodal distribution at $T = 300$ K (*times signs*); bimodal distribution at $T = 311$ K (*closed triangles*); and unimodal distribution at $T = 320$ K (*open squares*). Number of Monte Carlo cycles = 120,000. The cluster size is defined by the number of hydrocarbon chains belonging to the cluster.

for four different temperatures at the same DMPC/DSPC mole fraction of 64:36. In a 40×40 lattice there are 288 DSPC molecules at this mole fraction, and thus the size of a DSPC cluster, measured by the number of acyl chains forming the cluster, cannot be larger than 576. At a temperature of 220 K, at which the components are in gel phase, the size of DSPC clusters follow a bimodal distribution (see open circles in Fig. 1). The peak with a maximum at a cluster size of ~480 refers to the size distribution of the largest DSPC cluster of each snapshot (Sugar et al., 2001; Michonova-Alexova and Sugar, 2001), while the peak with a cusp-like maximum at cluster size 2 refers to the size distribution of all the DSPC clusters except the largest one. It is important to note that Figs.1 and 2 show only the lower part of the distributions up to frequencies of 0.0008. With decreasing cluster size the frequency increases continuously up to ~0.4–0.5 at cluster size 2.

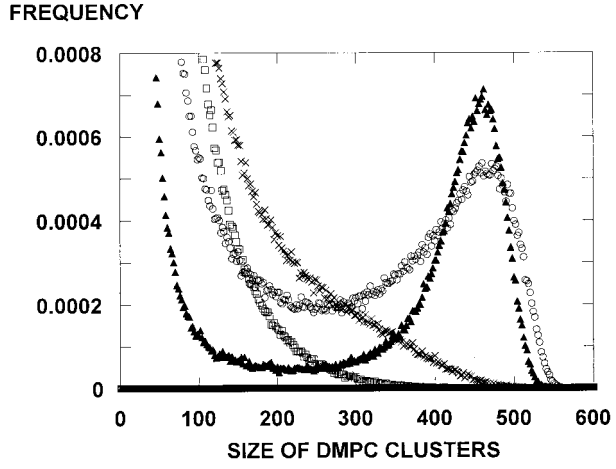

FIGURE 2 Size distributions of DMPC clusters in DMPC/DSPC (36:64) mixture. Bimodal distribution at $T = 220$ K (*open circles*); unimodal distribution at $T = 300$ K (*times signs*); bimodal distribution at $T = 315$ K (*closed triangles*); and unimodal distribution at $T = 330$ K (*open squares*). Number of Monte Carlo cycles = 120,000. The cluster size is defined by the number of hydrocarbon chains belonging to the cluster.

At the same mole fraction, with increasing temperature, the type of the distribution changes from bimodal to unimodal or from unimodal to bimodal three times. For example, at 300 K the distribution is unimodal (see times signs in Fig. 1). At a temperature of 311 K, a bimodal size distribution of the DSPC clusters is observed again with a local maximum at cluster size of 350 lattice points (see closed triangles in Fig. 1). At the even higher temperature of 320 K, the distribution is unimodal (see open squares in Fig. 1). Any further increase of the temperature does not change the type of the distribution.

At DMPC/DSPC mole fraction of 36:64, the type of the size distribution of DMPC clusters similarly alternates three times between unimodal and bimodal with increasing temperature (see Fig. 2). Examples of unimodal cluster size distributions are shown in Fig. 2 at 300 K (times signs) and 330 K (open squares); examples of bimodal cluster size distributions are shown at 220 K (open circles) and 315 K (closed triangles).

DISCUSSIONS

Relationships between cluster size population and distribution

The type of the size distribution of the compositional clusters is related to the type of population of cluster size. When the population is inhomogeneous, the size of the largest cluster of each snapshot scales with the size of the lattice (Michonova-Alexova and Sugar, 2001) and becomes infinite at an infinite lattice size, while the rest of the clusters remain small in the thermodynamic limit. However, when the population is homogeneous, all the clusters remain small with increasing lattice size. The threshold temperature separating the two populations is called the percolation threshold temperature (Stauffer and Aharony, 1992). In the case of an infinite lattice the cluster size distribution is unimodal if the population is homogeneous and bimodal when the population is inhomogeneous. In the case of a finite lattice, however, the relationship between the type of the population and the type of the respective cluster size distribution is not so straightforward. The distribution belonging to the homogeneous population is always unimodal. However, in the case of an inhomogeneous population, the type of distribution depends on the deviation of the actual temperature from the percolation threshold temperature. Far from the percolation threshold temperature, the distribution is bimodal. The second peak of the distribution is related to the

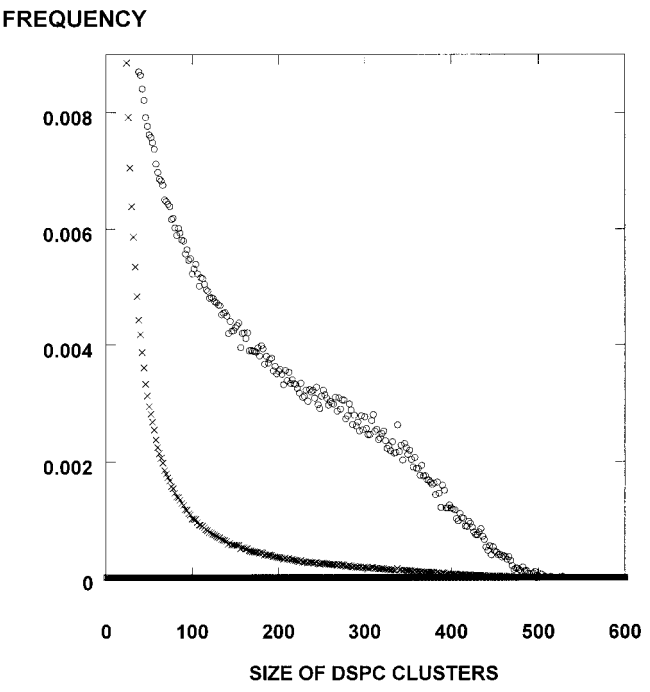

FIGURE 3 Two representations of the same normalized size distribution of DSPC clusters. (×) *f(s)* is plotted against *s*, where *f(s)* is the frequency of DSPC clusters of size *s*. (○) *sf(s)* is plotted against *s*, where *sf(s)* is the frequency of DSPC molecules situated in DSPC clusters of size *s*. DMPC/DSPC mole fraction = 64:36, T = 300 K; number of Monte Carlo cycles = 120,000.

size distribution of the largest cluster of each snapshot (Michonova-Alexova and Sugar, 2001), while the first, cusp-like peak is related to all the other clusters. When approaching the percolation threshold temperature, the second peak gets closer to the first peak, and they overlap each other more and more. At a certain temperature the second peak disappears, the distribution becomes unimodal, and only the shoulder of the cusp-like peak signifies that the respective cluster size population is inhomogeneous. Even closer to the percolation threshold temperature the second peak is overlapped by the first peak so much that there is not even a shoulder in the distribution. In this case, only the broadening of the distribution signifies the presence of a hidden second peak. One can emphasize the hidden second peak, which tends to belong to larger clusters than the first peak, by plotting $sf(s)$ against s, where $f(s)$ is the frequency of clusters of size s. As an example, Fig. 3 shows a cluster size distribution, $f(s)$ versus s, close to the percolation threshold temperature and the respective distorted distribution, $sf(s)$ versus s. The cluster size distribution is unimodal, without a shoulder. However, the appearance of the shoulder in the respective distorted distribution signifies the presence of a hidden second peak in the cluster size distribution.

We estimated the percolation threshold temperature as the temperature between two consecutive temperatures: at one of the temperatures the respective distorted distribution has a shoulder, while at the other temperature there is no shoulder. It is important to note that one can further emphasize the hiding second peak by plotting $s'' f(s)$ against s, where $n > 1$, but this would not change the estimated percolation threshold temperature significantly. As a result of a systematic search the percolation threshold temperatures were obtained at different DMPC/DSPC mole fractions. In the diagram of component separation the percolation threshold temperatures of the compositional clusters are plotted on the temperature/mole fraction plane (Fig. 4).

Diagram of component separation

The diagram of component separation (Fig. 4) contains two lines, the line of DSPC separation (marked by open triangles) and the line of DMPC separation (open circles), dividing the temperature/mole fraction plane into three regions. Between the two lines the populations of the cluster size are inhomogeneous for both DMPC and DSPC clusters. To the left of the line of DSPC separation, the population of the size of the DSPC and DMPC clusters are homogeneous and inhomogeneous, respectively. When approaching the line of DSPC separation from the right the peaks of the bimodal distribution of the DSPC clusters come closer to each other, and eventually the distribution becomes broad, unimodal. However, to the right of the line of DMPC separation the populations of the size of the DMPC and DSPC clusters are homogeneous and inhomogeneous, respectively. When approaching the line of DMPC separation from the left, the peaks of the bimodal distribution of the DMPC clusters come closer to each other, and eventually the distribution becomes broad, unimodal. The distributions in Fig. 1 may serve as examples for the above-described behaviors. In Fig. 1 the distributions are taken at the same mole fraction (36 mol% DSPC), but at different temperatures. It can be seen that the unimodal distribution of the DSPC clusters is broader at 300 K (times signs) than at 320 K (open squares). This is the case because at 300 K the line of DSPC separation is practically at 36 mol%, while at 320 K it is at 38 mol% DSPC, i.e., 2 mol% apart from 36 mol% (Fig. 4). By investigating the bimodal distributions one may notice that the two peaks are closer to each other at 311 K (closed triangles) than at 220 K (open circles). Again, this is the case because at 311 K the line of DSPC separation is at 29 mol% DSPC, i.e., only 7 mol% apart from 36 mol%, while at 220 K it is at 26 mol% DSPC, i.e., 10 mol% apart from 36 mol%.

The size distribution of compositional clusters in DMPC/DSPC mixtures was not measured, but the following observations in equimolar DMPC/DSPC mixtures are consistent with a bimodal size distribution. On one hand, neutron diffraction data showed very small DSPC clusters in the nanometer range (Gliss et al., 1998), while under similar conditions, an at least three orders of magnitude larger gel

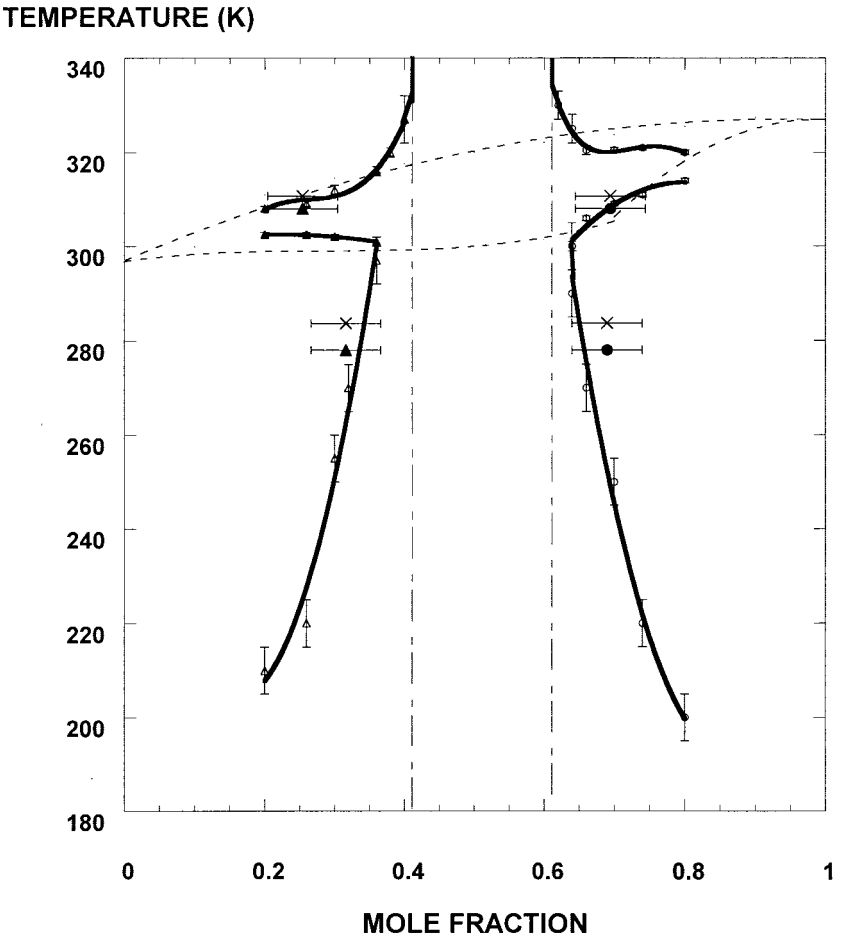

FIGURE 4 Component separation diagram of DMPC/DSPC bilayers. Heavy solid lines separate homogeneous and inhomogeneous populations of the cluster size of compositional clusters. *Open triangles:* line of separation for DSPC clusters; *open circles:* line of separation for DMPC clusters; *closed triangles* and *closed circles:* SANS data (Knoll et al., 1981) measured on DMPC-d_{54}/DSPC mixtures; *times signs:* adjusted SANS data for DMPC/DSPC mixtures; *dash-dotted lines:* component separation diagram in the case of the second model (model of independent double-chain molecules); *dashed line:* calculated DMPC/DSPC phase diagram. The onset and completion temperatures of the gel-to-fluid transition calculated at different DSPC mole fractions were used to construct the solidus and liquidus lines of the phase diagram (from Sugar et al., 1999).

cluster was visible in the gel-fluid mixed phase region by fluorescent microscope (Bagatolli and Gratton, 2000a). [More than one large gel cluster is present in the case of nonequilibrium distributions (Michonova-Alexova and Sugar, 2001). In equimolar DMPC/DSPC bilayer, the size of DSPC clusters is at least 70% of the size of the gel clusters because it follows from the phase diagram that the mole fraction of DSPC in the gel clusters is >70 mol%.]

Effects of interchain interactions on the diagram of component separation

The location and shape of the lines of component separation in the component separation diagram depend on the interchain interactions. Let us consider three different cases. *First*, let us assume that each component has only one chain and each chain is situated on a lattice point of a triangular lattice. We also assume that there are only nearest-neighbor interchain interactions and the interaction energies, E_{jk}^{mn}, are the same. In the rest of the paper this model is referred as the *first* model or model of independent chains. In the case of this model the two lines of component separation merge into one common vertical line at 50 mol% (50 mol% is the percolation threshold concentration in the case of noninteracting points on a triangular lattice (Stauffer and Aharony, 1992)). Thus, independently from the temperature at <50 mol% the population of the size of component 1 and 2 clusters is inhomogeneous and homogeneous, respectively, while the situation is opposite at >50 mol%. *Second*, similarly to our DMPC/DSPC bilayer model, it is assumed that nearest-neighbor pairs of chains of the same component are covalently connected, forming molecule 1 and molecule 2, while the interchain interactions remain component- and state-independent as in the *first* model. Thus, again, the components are randomly distributed. In the rest of the paper this model is referred as the *second* model or model of independent double-chain molecules. In this case the component separation diagram contains two vertical lines. The separation line of components 2 and 1 is situated at ~41 mol% and ~61 mol%, respectively (see dash-dotted lines in Fig. 4). Independently from the temperature, the homogeneous population of component 2 clusters becomes inhomogeneous at ~41 mol%, and not at 50 mol% as in the previous model. This is the case because the covalent bonds between the chains enforce strongly correlated lateral distributions of the chains of the same component, while the

distribution of the molecules is random. Thus the percolation of component 2 clusters, i.e., the formation of a large cluster scaling with the system size, takes place at a lower mole fraction than in the case of uncorrelated chains. The *third* model is our DMPC/DSPC model, where, besides the covalent link between the chains of each molecule, the interchain interactions depend on the type and state of the chains. The specificity of the interchain interaction is reflected in the temperature dependences of the lines of component separation in Fig. 4. The strongest temperature dependence can be seen in the gel-fluid coexistence region, where the lateral distribution of the molecules is determined by six different cooperativity parameters,

$$w_{jk}^{mn} = E_{jk}^{mn} - \frac{E_{jj}^{mn} + E_{kk}^{mn}}{2}$$

(see Table 1 in Sugar et al., 1999). [The calculated gel-fluid coexistence region is enclosed by dashed lines in Fig. 4. At every mole fraction the coexistence region is between the onset and completion temperature of the gel-to-fluid transition. The onset temperature is defined by the intercept of the baseline and a straight line fitted to the initial inflection point of the calculated excess heat capacity curve (Sugar et al., 1999).] Below the gel-fluid coexistence region, in the mostly gel region, the temperature dependence of the component separation lines is not so strong because only one cooperativity parameter, w_{12}^{gg}, defines the lateral distribution of the molecules (Sugar et al., 1999). Similarly, the temperature dependence is not so strong at the mostly fluid region, above the coexistence region, where only one cooperativity parameter, w_{12}^{ff}, defines the lateral distributions of the molecules (Sugar et al., 1999).

Random/nonrandom distribution of the components and the diagrams of component separation

At high temperatures, where $w_{12}^{ff}/kT \approx 0$, the *third* model and the *second* model become equivalent, i.e., from 330 K the lines of component separation become vertical at ~41 mol% and ~61 mol% DSPC (see Fig. 4), and from this temperature the lateral distribution of the components become random at any DMPC/DSPC mole fraction. To draw a conclusion about the randomness of the distribution of the components in DMPC/DSPC mixtures below 330 K, we compare the cluster size distributions of the *second* and *third* model at different mole fractions. At small mole fractions the cluster size distributions of the 2nd component, derived from the *second* and *third* model, are similar, unimodal distributions. Thus, similar to the distribution of the components in the *second model*, at low mole fractions DSPC (component 2) is randomly distributed in DMPC/DSPC mixtures, and if component 2 is randomly distributed, then component 1 (DMPC) should be randomly distributed, too. However, at the line of DSPC separation (left solid line in Fig. 4), the unimodal size distribution of the 2nd component, DSPC, becomes broader than that of the *second* model, i.e., the distribution of the DSPC and DMPC molecules starts to deviate from the random distribution. One can similarly realize that at high mole fractions the components are randomly distributed in the DMPC/DSPC mixtures, while at the line of DMPC separation the distribution of the components starts to deviate from random distribution.

Comparison of the diagram of component separation with the SANS data

Although there are numerous methods for the measurement of gel-fluid transition in lipid bilayers, such as DSC, Raman spectroscopy, dilatometry, densitometry, ESR, NMR, and fluorescence spectroscopy (see references in the Introduction), small-angle neutron scattering (SANS) has the unique advantage of being able to detect component separation when coupled with the use of deuterated lipids. By means of SANS, Knoll et al. (1981) determined the positions of the component separation lines for an equimolar DMPC-d_{54}/DSPC mixture at 278 K and 308 K (closed circles and closed triangles in Fig. 4). Within experimental error the observed data agree with the calculated ones. It is important to note, however, that the gel-to-fluid transition temperature of DMPC-d_{54} is 5.7 K lower than the transition temperature of DMPC, and thus the experimental phase diagram of DMPC-d_{54}/DSPC (Schmidt and Knoll, 1986) is slightly different from that of the DMPC/DSPC (Knoll et al., 1981). Based on the differences in the phase diagrams, we adjusted the SANS data to estimate the position of the lines of component separation in the case of DMPC/DSPC mixtures (see times signs in Fig. 4). These adjusted SANS data are also in agreement with the calculated values.

The other important finding of the SANS measurement was that the components are not randomly distributed above the liquidus line at 50 mol% DSPC (Knoll et al., 1981, 1983). At 50 mol% DSPC SANS measurements were performed at three different temperatures above the liquidus line, i.e., above 317 K. Nonrandom distribution was found at 318 K and 321.5 K, but the distribution was random at 331 K. This finding is also in agreement with the calculated component separation diagram in Fig. 4. According to our calculations, above 330 K random distribution of the components is attained at any DMPC/DSPC mole fraction, i.e., above the temperature where the component separation lines (heavy lines in Fig. 4) merge with the dash-dotted lines at 41 mol% and 61 mol%.

SANS experiments, performed at 40 mol% DSPC, showed that the distribution of the components was almost random at the liquidus line. This finding is also in rather good agreement with the calculated results. According to Fig. 4, at 34 mol% DSPC the liquidus curve intersects the

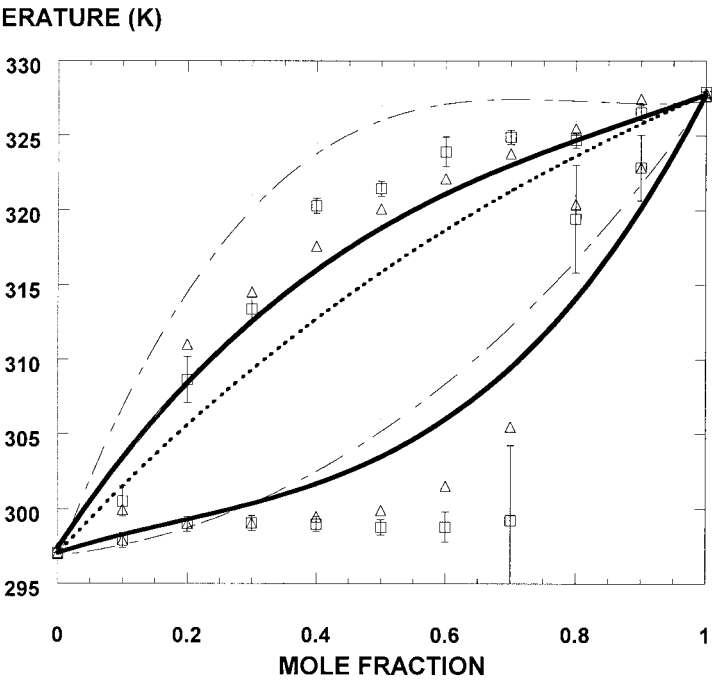

FIGURE 5 State separation diagram of DMPC/DSPC mixtures. Heavy solid lines separate the homogeneous and inhomogeneous populations of the size of gel/fluid clusters. The line at higher and lower temperature is the line of separation for gel and fluid state clusters, respectively. *Dotted line:* state separation diagram for the model of independent chains (*first* model); *dash-dotted line:* state separation diagram for the model of independent double-chain molecules (*second* model); *open squares:* experimental onset and completion temperatures of the gel-to-fluid transition at different DSPC mole fractions (from Sugar et al., 1999); *open triangles:* calculated onset and completion temperatures of the gel-to-fluid transition at different DSPC mole fractions (from Sugar et al., 1999).

DSPC separation line, i.e., at and above the intersect the DSPC distribution should be random. Knoll et al. (1983) explained the nonrandom distribution of the components above the liquidus line in equimolar DMPC/DSPC mixture by means of critical demixing. According to our model the gel-to-fluid transition is a continuous transition at every mole fraction (Sugar et al., 1999; Sugar and Biltonen, 2000), i.e., the system is above the critical temperature, and thus the nonrandom distribution of the components cannot be explained by critical demixing.

Off-plane reactions and component separation

Off-plane or membrane surface reaction takes place when one of the reactants is located at the membrane surface, while the other reactant is in the solution around the membrane, and they react on the membrane surface, e.g., substrate binding on a membrane receptor. Let us assume that the off-plane reactant reacts specifically with the polar head of one of the lipid components of the membrane. [Note that DMPC/DSPC mixture is not a good example because the polar heads of the components are the same.] The apparent equilibrium poise of the off-plane reaction may markedly change at the percolation threshold temperature of the lipid component participating in the surface reaction. When the cluster size distribution of this lipid component is unimodal, as many off-plane reactions may take place as many small clusters are present. With a bimodal distribution of the specific membrane component, a considerable proportion of the specific component forms the largest cluster. However, the number of substrate molecules binding simultaneously on the largest cluster can be severely constrained by the excluded volume interaction between the substrates.

Diagram of state separation

By using the DMPC/DSPC bilayer model one can generate the size distributions of gel state and fluid state clusters at different points of the temperature/mole fraction plane. As an example, Fig. 3 in Sugar et al. (2001) shows the size distributions of fluid clusters of equimolar DMPC/DSPC bilayers at three different temperatures. The distribution is unimodal at 302 K (Fig. 3 *A*), bimodal at 306 K (Fig. 3 *C*), and possesses a shoulder at 305.3 K (Fig. 3*B*). Similarly to the compositional clusters, the population of the size of the gel/fluid state clusters is either homogeneous or inhomogeneous, and the percolation threshold temperature separates these two populations. After generating the size distributions of fluid clusters of equimolar DMPC/DSPC bilayers at several temperatures, one can estimate the percolation threshold temperature, ~303K, by using the method of distorted distributions (see Relationships between cluster size population and distribution). In the same way, one can get the percolation threshold temperatures for both gel and fluid clusters at different DMPC/DSPC mole fractions, and construct a state separation diagram by plotting the percolation threshold temperatures at the respective mole fractions (Fig. 5). The state separation diagram contains two lines (heavy lines in Fig. 5): the line of gel separation at higher temperatures and the line of fluid separation at lower temperatures. Above the line of gel separation the population of the size of the gel and fluid state clusters are

homogeneous and inhomogeneous, respectively. Below the line of fluid separation the population of the size of the fluid and gel state clusters are homogeneous and inhomogeneous, respectively. Between the lines of gel and fluid separation the population of the cluster size is inhomogeneous for both gel and fluid state clusters. When approaching the line of gel separation from below, the peaks of the bimodal distribution of the size of the gel clusters come closer to each other, and eventually the distribution becomes broad, unimodal. Similarly, when approaching the line of fluid separation from above, the peaks of the bimodal distribution of the size of the fluid clusters come closer to each other, and eventually the distribution becomes broad, unimodal.

Effects of interchain interactions on the diagram of state separation

The location and shape of the lines of state separation in the state separation diagram depend on the interchain interactions. Let us consider again the three models discussed in the case of the component separation diagram.

In the case of the *first model*, the model of independent chains, the state separation diagram can be calculated analytically (see the Appendix). In this case there is only one state separation line (dotted line in Fig. 5). Above the line the population of the size of gel and fluid clusters is homogeneous and inhomogeneous, respectively, while below the line the population of the size of gel and fluid clusters is inhomogeneous and homogeneous, respectively. There is no region where the population is inhomogeneous for both gel and fluid clusters.

In the case of the *second model*, the model of independent double-chain molecules, the state separation diagram (dash-dotted lines in Fig. 5) can be obtained by simulation. In the simulations our DMPC/DSPC model was utilized by taking zero for every cooperativity parameter, $w_{jk}^{mn} = 0$ *cal/mol · chain*. The state separation diagram of *the second model* has two separation lines. It is qualitatively different from that of the *first model* solely because of the covalent bonds between the pairs of chains. The difference between the state separation diagram of the *second* and *third* model is only quantitative and is caused by the introduction of non-zero cooperativity parameters.

Random/nonrandom distribution of the fluid/gel chains and the state separation diagrams

To draw a conclusion about the randomness of the distribution of the fluid/gel chains in DMPC/DSPC mixtures we compare the cluster size distributions of the *second* and *third* models at different temperatures. At low temperatures the size distribution of the fluid state clusters derived from the *second* and *third* models are similar, unimodal distributions. Thus, as with the distribution of the fluid chains in the *second model*, at low temperatures the fluid state chains (of the *third model*) are randomly distributed in DMPC/DSPC mixtures, and if the fluid chains are randomly distributed, then the gel state chains should be randomly distributed, too. However, at the line of fluid state separation of the *third model* (the lower solid line in Fig. 5), the unimodal size distribution of the fluid clusters (of the *third model*) becomes broader than that of the *second model*, i.e., the distribution of the fluid/gel state chains of the *third model* starts to deviate from the random distribution.

At high temperatures the size distribution of the gel state clusters, derived from the *second* and *third model*, are similar, unimodal distributions. Thus, at high temperatures the gel state chains are randomly distributed in DMPC/DSPC mixtures, and thus the fluid chains will be randomly distributed, too. However, at the line of gel state separation of *the second model* (the upper dash-dotted line in Fig. 5) the unimodal size distribution of the gel clusters (of the *second model*) becomes broader than that of the *third model*, i.e., the distribution of the gel/fluid chains of the *third model* starts to deviate from the random distribution of the *second model*.

Comparison of different estimates of the percolation threshold temperatures

So far, percolation threshold temperatures were estimated by analyzing the cluster size distributions. In the case of a finite lattice, one can also estimate the percolation threshold temperature by constructing the percolation frequency curve. During the Monte Carlo simulation of DMPC/DSPC mixtures, a snapshot is percolated if a cluster spans the lattice from the top to the bottom or from the left to the right edge. The frequency of percolated snapshots is the percolation frequency. In Fig. 6, *A* and *B*, the percolation frequencies of fluid and gel clusters are plotted against the temperature at five different mole fractions. By means of a percolation frequency curve, the percolation threshold temperature of the respective clusters can be estimated. A straight line should be fitted to the inflection point of the percolation frequency curve. Its intercept with the zero frequency line gives an estimation of the percolation threshold temperature (see long vertical bars in Fig. 6). The position of these percolation threshold temperatures can be compared with the estimates obtained from the analysis of the size distributions of fluid and gel clusters (see short vertical bars connected to the respective long vertical bars in Fig. 6). As a consequence of the finite size effects the two different methods, the analysis of percolation frequency curves and the analysis of cluster size distributions, result in different estimates for the percolation threshold temperature.

The percolation threshold temperature obtained from the analysis of the distributions is located at the beginning of the initial tail of the percolation frequency curve, i.e., where

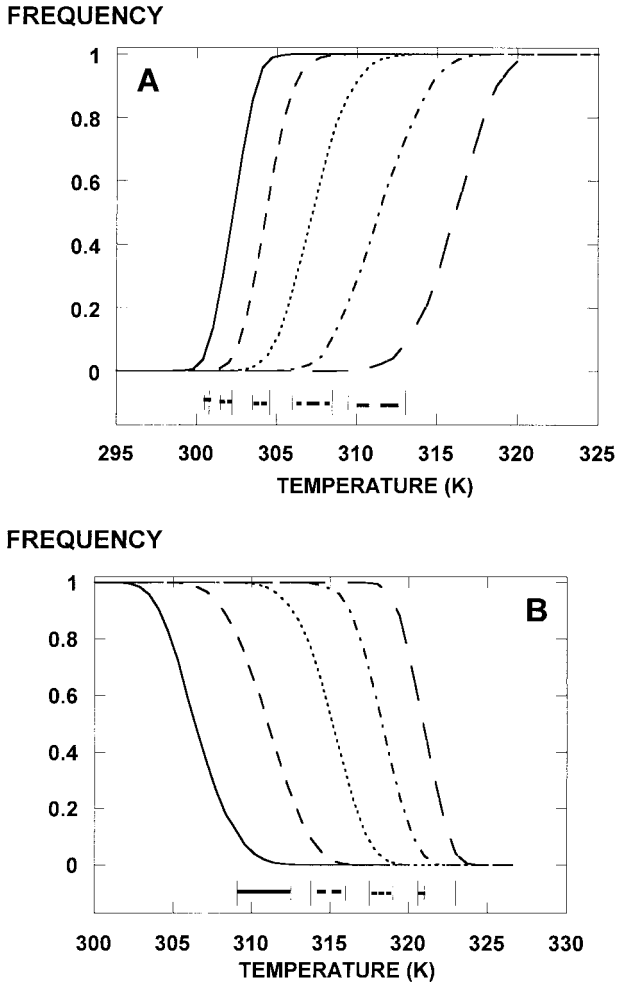

FIGURE 6 Percolation frequency curves of gel and fluid clusters in DMPC/DSPC mixtures. (*A*) Calculated percolation frequency of fluid clusters versus temperature. (*B*) Calculated percolation frequency of gel clusters versus temperature. *Long vertical bar:* percolation threshold temperature, estimated from percolation frequency curve. *Short vertical bar:* percolation threshold temperature, estimated from cluster size distributions. Vertical bars, one short and one long, belonging to the same mole fraction, are interconnected with a horizontal line. DMPC/DSPC mole fractions are marked by solid line (70:30), short-dashed line (60:40), dotted line (50:50), dash-dotted line (40:60), and long-dashed line (30:70).

percolated snapshots appear with almost zero frequency. At infinite lattice size this initial tail of the percolation frequency curve disappears and the two different estimates of the percolation threshold temperature become equal to each other.

In-plane reactions and state separation. Comparison to the FRAP data.

In-plane membrane reactions take place in the fluid regions, where the lateral diffusion of the molecules is more than three orders of magnitudes faster than in the gel regions (Kapitza et al., 1984). Thompson et al. (1995) pointed out that at the percolation threshold temperature (assumed to be the same for gel and fluid clusters) the apparent equilibrium poise and rates of in-plane reactions may change significantly. As they argued, this is the case because passing across the percolation threshold temperature changes the reaction system to one that can achieve global equilibrium if the reaction cluster is continuous or consists of many isolated systems, each individually at equilibrium. It is important to note that the respective calculations (Melo et al., 1992) assume constant cluster size and static cluster connectedness, while, according to our DMPC/DSPC model, the cluster size distribution is broad (see Fig. 3 in Sugar et al., 2001) and the connectedness of the clusters is dynamic (see Fig. 6). Fig. 5 shows the line of fluid state separation of DMPC/DSPC mixtures, where significant change in the in-plane chemical reactions can be expected. This line, however, does not coincide with the line of gel state separation, i.e., the percolation threshold temperatures of gel and fluid clusters are different at the same DSPC mole fraction. We note that the two percolation threshold temperatures coincide only in the case of the *first* model, the model of independent chains. FRAP threshold temperature, signifying the onset of long-range diffusion within the fluid phase region (Vaz et al., 1989), is assumed to be related to percolation threshold temperature. FRAP threshold temperatures were measured at different DMPC/DSPC mole fractions by Vaz et al. (1989). Recently, by using the same DMPC/DSPC model we found a strong, positive correlation between the FRAP threshold temperatures, measured at different DMPC/DSPC mole fractions, and the percolation threshold temperatures of gel clusters, estimated from the percolation frequency curves (Sugar et al., 1999, 2001). However, the correlation was weak with the percolation threshold temperatures of the fluid clusters. It was pointed out that in the time frame of the FRAP experiments, the largest gel cluster efficiently blocks the long-range diffusion of the molecules in the fluid regions if the percolation frequency of the largest gel cluster is >0.36. As it was mentioned above, a marked change in the in-plane chemical reactions is anticipated not at the FRAP threshold, which is close to the percolation threshold of gel clusters, but close to the percolation threshold of fluid clusters.

On the type of the DMPC/DSPC phase diagram

While state and component separation diagrams are defined by the percolation threshold temperatures of the gel/fluid and compositional clusters, experimental phase diagrams are defined by the onset and completion temperatures of the gel-to-fluid transition. In addition, the state separation diagrams in Fig. 5 show both the experimental and calculated onset and completion temperatures of the gel-to-fluid transition at different mole fractions (see open squares and triangles, respectively). These data were obtained from the analysis of the experimental and calculated excess heat

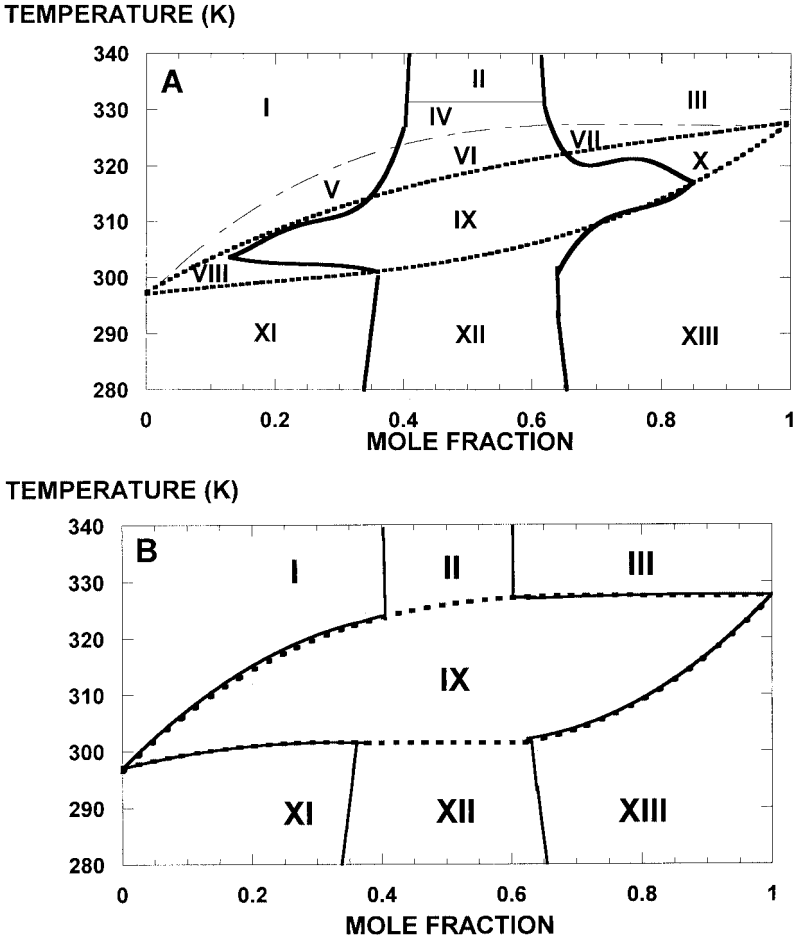

FIGURE 7 Combined component and state separation diagrams. (*A*) Combined component and state separation diagram of DMPC/DSPC mixtures. *Heavy solid lines:* lines of component separation; *heavy dotted lines:* lines of state separation; *thin dash-dotted line:* gel state separation line in the case of independent double-chain molecules (*second model*). Above the thin solid line the DMPC/DSPC model (*third* model) and the model of independent double chain molecules (*second model*) result in the same percolation threshold temperatures of the compositional clusters. (*B*) Illustration of the construction of a peritectic phase diagram from the combination of a component and state separation diagram. *Heavy solid lines:* lines of component separation; *heavy dotted lines:* lines of state separation. The properties of the regions marked by Roman numerals are listed in Table 1.

capacity curves of DMPC/DSPC mixtures (Sugar et al., 1999). The onset and completion temperatures define the solidus and liquidus line of the experimental phase diagram of DMPC/DSPC, respectively. The quantitative agreement between the experimental and calculated onset/completion temperatures shows that our model correctly calculates the experimental phase diagram of DMPC/DSPC bilayers.

Because of the experimental errors, it was debated whether the solidus line has a horizontal section, i.e., the type of the phase diagram is peritectic or not (Mabrey and Sturtevant, 1976; Wilkinson and Nagle, 1979; Knoll et al., 1981, 1983; Schmidt and Knoll, 1986). Eventually the SANS data showed that the distribution of the components below the solidus curve (from 30 to 70 mol%) deviates from a random distribution and concluded that the type of the phase diagram is peritectic. Although our simulations are in quantitative agreement with the SANS data, we cannot make the same conclusion. This is the case because, according to our model, the gel-to-fluid transition in DMPC/DSPC mixtures is a continuous transition at every mole fraction (Sugar et al., 1999), and in a strict theoretical sense one can define solidus and liquidus lines of a phase diagram only in the case of first-order transitions (Sugar and Biltonen, 2000).

It is important to note here that in the case of DMPC-d_{54}/DPPC mixtures, SANS data showed random distribution of the components below and above the experimental solidus and liquidus line, respectively, while the distributions of the components were not random between these lines (Knoll et al., 1981). By means of the result of Knoll et al. one can predict the diagram of component separation for DMPC/DPPC mixtures. Below and above the solidus and liquidus line, respectively, the lines of component separation are vertical and located at ~41% and ~61% mole fraction (coinciding with the dash-dotted line in Fig. 4). At the gel-fluid mixed phase region, however, the lines of component separation deviate from these vertical lines, similarly to the component separation diagram of DMPC/DSPC in the gel-fluid mixed phase region (see Fig. 4). [Note that in the case of DMPC/DSPC mixture, below the solidus line the component separation lines get close to the dash-dotted line. The distribution of the components becomes close to, but does not attain, random distribution (see Fig. 4).]

Comparison of the diagrams of component separation and state separation

In Fig. 7 *A* the combined diagram of state and component separation is shown. The lines of gel and fluid state sepa-

TABLE 1 Properties of the regions in the combined diagram of state and component separation

Code Number Region	Type of Population of the Size of Gel/Fluid Clusters		Lateral Distribution of Gel/Fluid Chains	Type of Population of the Size of Compositional Clusters		Lateral Distribution of the Components
	Gel	Fluid		DSPC	DMPC	
I	Homog.	Inhomog.	Random	Homog.	Inhomog.	Random
II	Homog.	Inhomog.	Random	Inhomog.	Inhomog	Random
III	Homog.	Inhomog.	Random	Inhomog.	Homog.	Random
IV	Homog.	Inhomog.	Random	Inhomog.	Inhomog	Nonrandom
V	Homog.	Inhomog.	Nonrandom	Homog.	Inhomog.	Random
VI	Homog.	Inhomog.	Nonrandom	Inhomog.	Inhomog.	Nonrandom
VII	Homog.	Inhomog.	Nonrandom	Inhomog.	Homog.	Random
VIII	Inhomog.	Inomog.	Nonrandom	Homog.	Inhomog.	Random
IX	Inhomog.	Inhomog.	Nonrandom	Inhomog.	Inhomog.	Nonrandom
X	Inhomog.	Inhomog.	Nonrandom	Inhomog.	Homog.	Random
XI	Inhomog.	Homog.	Random	Homog.	Inhomog.	Random
XII	Inhomog.	Homog.	Random	Inhomog.	Inhomog.	Nonrandom
XIII	Inhomog.	Homog.	Random	Inhomog.	Homog.	Random

ration (heavy dashed lines) are confined to the temperature interval (T_1, T_2), where T_1 and T_2 are the temperature of gel-to-fluid transition of pure DMPC and DSPC bilayer, respectively. The temperature region for the lines of component separation (heavy solid lines) is not confined, but they are confined to intermediate DMPC/DSPC mole fractions. We note that the component separation lines at <20 mol% and above 80 mol% have been extrapolated from the component separation lines in Fig. 4. The dash-dotted line is the gel state separation line of the *second model*. Above the thin, horizontal, solid line, the size distribution of the compositional clusters are the same for the *second* and *third model* at every mole fraction.

As mentioned in the previous section, in a strictly theoretical sense one cannot define solidus and liquidus lines of DMPC/DSPC bilayers in the temperature/mole fraction plane because the gel-to-fluid transition is not a first-order transition. The combined diagram of component and state separation, however, provides a theoretically proper characterization of the DMPC/DSPC system. The lines of component and state separation divide the temperature/mole fraction plane into 13 regions marked by Roman numerals in Fig. 7 *A*. These regions are characterized by different populations of the size of the gel/fluid and compositional clusters, and by different lateral distributions of the components and gel/fluid chains (see Table 1).

Our notion is that in the case of first-order phase transition the combined diagram of state and component separation is degenerated into a phase diagram, i.e., certain sections of the state and component separation lines merge into each other and thus the phase diagram divides the temperature/mole fraction plane into fewer regions. As an example, Fig. 7 *B* shows how a peritectic phase diagram can be constructed from a state and a component separation diagram. This combined diagram separates only seven regions in the temperature/mole fraction plane. The properties of these regions are listed in Table 1.

CONCLUSIONS

A simple two-state, two-component Ising-type model of DMPC/DSPC bilayers has been capable of calculating the excess heat capacity curves, FRAP threshold temperatures, most frequent center-to-center distances between DSPC clusters and fractal dimensions of gel clusters in quantitative agreement with the respective experimental data. The equilibrium size distributions of the compositional clusters or gel/fluid clusters are either unimodal or bimodal, depending on the temperature and mole fraction. Many small, nanometer-size clusters are present when the size distribution is unimodal, while in the case of bimodal distribution, one large cluster, of a size comparable with the bilayer's size, coexists with the small ones. Diagrams of component or state separation are constructed by plotting the percolation threshold temperatures of compositional or fluid/gel state clusters, respectively, in the temperature/mole fraction plane. The calculated component separation diagram shows a nonrandom lateral distribution of the components below 57°C, i.e., not only in the gel-fluid mixed phase region, but also in parts of the all-fluid and all-gel regions. This result is in quantitative agreement with the small-angle neutron scattering data. A combined diagram of component and state separation is constructed to characterize the lateral distribution of components and gel/fluid state chains in the DMPC/DSPC mixture. While theoretical phase diagrams of two-component mixtures can be constructed only in the case of first-order transitions, combined state and component separation diagrams can be created in the case of any type of transitions, and even in the lack of transition.

APPENDIX

Let us assume that in a two-component monolayer of a bilayer each component has only one chain and each chain is situated on a lattice point of a triangular lattice. We also assume that there are only nearest-neighbor

interchain interactions and the interaction energies, E_{jk}^{mn}, are the same. With these assumptions the probability that a chain of component j is in fluid state is:

$$p_j^f = \frac{\exp - (\Delta E_j - T\Delta S_j)/RT}{1+\exp - (\Delta E_j - T\Delta S_j)/RT} = \frac{q_j}{1+q_j}, \quad \text{(A1)}$$

where R, ΔE_j, and ΔS_j are the Boltzmann constant, the transition energy, and transition entropy per chain, respectively, in a pure j component bilayer. The average number of chains in fluid state is:

$$\langle N^f \rangle = N_1 p_1^f + N_2 p_2^f = N[(1 - X_2)p_1^f + X_2 p_2^f], \quad \text{(A2)}$$

where X_2 [$= N_2/N$] is the mole fraction of component 2. At the percolation threshold concentration of the fluid clusters $\langle N^f \rangle / N = ½$ (50% is the percolation threshold concentration in the case of noninteracting points on a triangular lattice (Stauffer and Aharony, 1992)). After substituting the percolation threshold concentration into Eq. A2 we get:

$$(1 - X_2)\frac{1 - q_1}{1 + q_1} + X_2 \frac{1 - q_2}{1 + q_2} = 0. \quad \text{(A3)}$$

This is an implicit equation for the percolation threshold temperature, T_{perc}, at mole fraction X_2. Equation A3 has explicit solutions only for the pure, one-component cases: T_{perc} ($X_2 = 0$) = $\Delta E_1/\Delta S_1$ and T_{perc} ($X_2 = 1$) = $\Delta E_2/\Delta S_2$. By using the parameters of the DMPC/DSPC model: ΔE_1 = 3028 cal/mol.chain, ΔE_2 = 5250 cal/mol.chain, ΔS_1 = 10.19378 cal/mol.chain/deg, ΔS_2 = 16.01689 cal/mol.chain/deg listed in Table 1 in Sugar et al. (1999), the numerical solution of Eq.A3 provides the percolation threshold temperatures at different mole fractions (see dotted line in Fig. 5)

We acknowledge one of the reviewers for advising the method of distorted distributions to estimate percolation threshold temperatures. We also thank Linda Rolnitzky for proofreading the manuscript. Dr. Sugar acknowledges Lilian Garner's generous support.

This work was supported by Pfizer, Inc.

REFERENCES

Bagatolli, L. A., and E. Gratton. 2000a. Two-photon fluorescence spectroscopy of coexisting lipid domains in giant unilamellar vesicles of binary phospholipid mixtures. *Biophys. J.* 78:290–305.

Bagatolli, L. A., and E. Gratton. 2000b. A correlation between lipid domain shape and binary phospholipid mixture composition in free standing bilayers: a two-photon fluorescence microscopy. *Biophys. J.* 79: 434–447.

Bergelson, L. O., K. Gawrisch, J. A. Feretti, and R. Blumenthal. 1995. Special Issue on Domain Organization in Biological Membranes. *Mol. Membr. Biol.* 12:1–162.

Binder, K., and D. Stauffer. 1987. Monte Carlo studies of "random" systems. *In* Applications of the Monte Carlo Method in Statistical Physics, Chapter 8. K. Binder, editor. Springer-Verlag, Berlin, Heidelberg, New York, Tokyo.

Brown, D. A., and E. London. 1998. Structure and origin of ordered lipid domains in biological membranes. *J. Membr. Biol.* 164:103–114.

Brumbaugh, E. E., and C. Huang. 1992. Parameter estimation in binary mixtures of phospholipids *Methods Enzymol*. 210:521–539.

Brumbaugh, E. E., M. Johnson, and C. Huang. 1990. Nonlinear least squares analysis of phase diagrams for nonideal binary mixtures of phospholipids. *Chem. Phys. Lipids.* 52:69–78.

Brumm, T., K. Jørgensen, O. G. Mouritsen, and T. Bayerl. 1996. The effect of increasing membrane curvature on the phase transition and mixing behavior of a dimyristoyl-*sn*-glycero-3-phosphatidylcholine/distearoyl-*sn*-glycero-3-phosphatidylcholine lipid mixture as studied by Fourier transform infrared spectroscopy and differential scanning calorimetry. *Biophys. J.* 70:1373–1379.

Dibble, A. R. G., A. K. Hinderliter, J. J. Sando, and R. L. Biltonen. 1996. Lipid lateral heterogeneity in phosphatidylcholine/phosphatidylserine/diacylglycerol vesicles and its influence on protein kinase C activation. *Biophys. J.* 71:1877–1890.

Evans, E., and R. Kwok. 1982. Mechanical calorimetry of large dimyristoylphosphatidylcholine vesicles in the phase transition region. *Biochemistry*. 21:4874–4879.

Glaser, M., W. S. Wanaski, C. A. Buser, V. Boguslavsky, W. Rashidzada, A. Morris, M. Rebecci, S. F. Scarlata, L. W. Runnels, G. D. Prestwich, J. Chen, A. Aderem, J. Ahn, and S. McLaughlin. 1996. A myristoylated alanine-rich C kinase substrate (MARCKS) produces reversible inhibition of phospholipase C by sequestering phosphatidylinositol 4,5-bisphosphate in lateral domains. *J. Biol. Chem.* 271:26187–26193.

Gliss, C., H. Clausen-Schaumann, R. Gunther, S. Odenbach, O. Randl, and T. M. Bayerl. 1998. Direct detection of domains in phospholipid bilayers by grazing incidence diffraction of neutrons and atomic force microscopy. *Biophys. J.* 74:2443–2450.

Heimburg, T. 2000. A model for the lipid pretransition: coupling of ripple formation with the chain-melting transition. *Biophys. J.* 78:1154–1165.

Honger, T., K. Jørgensen, R. L. Biltonen, and O. G. Mouritsen. 1996. Systematic relationship between phospholipase A2 activity and dynamic lipid bilayer microheterogeneity. *Biochemistry*. 35:9003–9006.

Huang, K. 1963. Statistical Mechanics. Wiley, New York. 336.

Hui, S. W. 1976. Tilting of hydrocarbon chains in a single bilayer of phospholipid. *Chem. Phys. Lipids.* 16:9–18.

Hui, S. W., R. Viswanathan, J. A. Zasadzinski, and J. N. Israelachvilli. 1995. The structure and stability of phospholipid bilayers by atomic force microscopy. *Biophys. J.* 68:171–178.

Hwang, J., L. A. Gheber, L. Margolis, and M. Edidin. 1998. Domains in cell plasma membranes investigated by near-field scanning optical microscopy. *Biophys. J.* 74:2184–2190.

Ipsen, J. H., and O. G. Mouritsen. 1988. Modeling with phase equilibria in two-component membranes of phospholipids with different acyl-chain lengths. *Biochim. Biophys. Acta.* 944:121–134.

Ising, E. 1925. Beitrag zur Theorie des Ferromagnetismus. *Zeitschrift für Physik* 31:253–258.

Jan, N., T. Lookman, and D. Pink. 1984. On computer simulation methods used to study models of two-component lipid bilayers. *Biochemistry*. 23:3227–3231.

Janiak, M. J., D. M. Small, and G. G. Shipley. 1979. Temperature and compositional dependence of the structure of hydrated dimyristoyl lecithin. *J. Biol. Chem.* 254:6068–6078.

Jørgensen, K., M. Sperotto, O. G. Mouritsen, J. Ipsen, and M. Zuckermann. 1993. Phase equilibria and local structure in binary lipid bilayers. *Biochim. Biophys. Acta.* 1152:135–142.

Jutila, A., and P. K. J. Kinnunen. 1997. Novel features of the main transition of dimyristoylphosphocholine bilayers revealed by fluorescence spectroscopy. *J. Phys. Chem. B.* 101:7635–7640.

Kapitza, H. G., D. A. Ruppel, H. J. Galla, and E. Sackmann. 1984. Lateral diffusion of lipids and glycophorin in solid phosphatidylcholine bilayers. The role of structural defects. *Biophys. J.* 45:577–587.

Knoll, W., K. Ibel, and E. Sackmann. 1981. Small-angle neutron scattering study of lipid phase diagrams by the contrast variation method. *Biochemistry*. 20:6379–6383.

Knoll, W., G. Schmidt, E. Sackmann, and K. Ibel. 1983. Critical demixing in fluid bilayers of phospholipid mixtures. A neutron diffraction study. *J. Chem. Phys.* 79:3439–3442.

Koynova, R., and M. Caffrey. 1998. Phases and phase transitions of the phosphatidylcholines. *Biochim. Biophys. Acta.* 1376:91–145.

Langelet, C., A. M. Bernard, P. Drevot, and H. T. He. 2000. Membrane rafts and signaling by the multichain immune recognition receptors. *Curr. Opin. Immunol.* 12:250–255.

Leidy, C., W. F. Wolkers, K. Jørgensen, O. G. Mouritsen, and J. H. Crowe. 2001. Latelar organization and domain formation in a two-component lipid membrane system. *Biophys. J.* 80:1819–1828.

Lu, D., I. Vavasour, and M. R. Morrow. 1995. Smoothed acyl chain orientational order parameter profiles in DMPC-DSPC mixtures: a ^{2}H-NMR study. *Biophys. J.* 68:574–583.

Mabrey, S., and J. M. Sturtevant. 1976. Investigation of phase transitions of lipids and lipid mixtures by high sensitivity differential scanning calorimetry. *Proc. Natl. Acad. Sci. USA.* 73:3862–3866.

Melo, E. C. C., I. M. G. Lourtie, M. B. Sankaram, T. E. Thompson, and W. L. C. Vaz. 1992. Effects of domain connection and disconnection on the yields of in-plane biomolecular reaction in membranes. *Biophys. J.* 63:1506–1512.

Mendelsohn, R., and J. Maisano. 1978. Use of deuterated phospholipids in Raman spectroscopic studies of membrane structure. I. Multilayers of dimyristoylphosphatidylcholine (and its *d*54 derivative) with distearoylphosphatidylcholine. *Biochim. Biophys. Acta.* 506:192–201.

Metropolis, M., A. W. Rosenbluth, M. N. Rosenbluth, and A. N. Teller. 1953. Equation of state calculations by fast computing machines. *J. Chem. Phys.* 21:1087–1092.

Michonova-Alexova, E. I., and I. P. Sugar. 2001. Size distribution of gel and fluid clusters in DMPC/DSPC lipid bilayers. A Monte Carlo simulation study. *J. Phys. Chem. B.* 105:10076–10083.

Mouritsen, O. G., and K. Jørgensen. 1997. Small scale lipid-membrane structure: simulation versus experiment. *Curr. Opin. Struct. Biol.* 7:518–527.

Mukherjee, S., T. T. Soe, and F. R. Maxfield. 1999. Endocytic sorting of lipid analogues differing solely in the chemistry of their hydrophobic tails. *J. Cell Biol.* 144:1271–1284.

Muresan, A. S., H. Diamant, and K. Y. C. Lee. 2001. Effect of temperature and composition on the formation of nanoscale compartments in phospholipid membranes. *J. Am. Chem. Soc.* 123:6951–6952.

Nielsen, L. K., A. Vishnyakov, K. Jørgensen, T. Bjørnholm, and O. G. Moritsen. 2000. Nanometer scale structure of fluid lipid membranes. *J. Phys. Condens. Matter.* 12:A309–A314.

Norris, V., and M. S. Madsen. 1995. Autocatalic gene expression occurs via transertion and membrane domain formation and underlies differentiation in bacteria: a model. *J. Mol. Biol.* 253:739–748.

Pedersen, S., K. Jørgensen, T. Bækmark, and O. G. Mouritsen. 1996. Indirect evidence for lipid domain formation in the transitional region of phospholipid bilayers by two-probe fluorescence energy transfer. *Biophys. J.* 71:554–560.

Piknova, B., D. Marsh, and T. E. Thompson. 1996. Fluorescence-quenching study of percolation and compartmentalization in two-phase lipid bilayers. *Biophys. J.* 71:892–897.

Priest, R. 1980. Landau phenomenological theory of one and two component phospholipid bilayers. *Mol. Cryst. Liq. Cryst.* 60:167–184.

Risbo, J., M. Sperotto, and O. G. Mouritsen. 1995. Theory of phase equilibria and critical mixing points in binary lipid bilayers. *J. Chem. Phys.* 103:3643–3656.

Sankaram, M. B., D. Marsh, and T. E. Thompson. 1992. Determination of fluid and gel domain sizes in 2-component, 2-phase lipid bilayers: an electron-spin-resonance spin label study. *Biophys. J.* 63:340–349.

Sankaram, M. B., and T. E. Thompson. 1992. Deuterium magnetic resonance study of phase equilibria and membrane thickness in binary phospholipid mixed bilayers. *Biochemistry.* 31:8258–8268.

Scheiffele, P., A. Tietveld, T. Wilk, and K. Simons. 1999. Influenza viruses select ordered lipid domains during budding from the plasma membrane. *J. Biol. Chem.* 274:2038–2044.

Schmidt, G., and W. Knoll. 1986. On the peritectic phase behavior of dimyristoyllecithin/distearoyllecithin mixtures. A densitometric study. *Chem. Phys. Lipids.* 39:329–339.

Schram, V., H.-N. Lin, and T. E. Thompson. 1996. Topology of gel-phase domains and lipid mixing properties in phase-separated two-component phosphatidylcholine bilayers. *Biophys. J.* 71:1811–1822.

Scott, H. L., E. Jacobson, and S. Subramaniam. 1998. Simulation of lipid membranes with atomic resolution. *Comp. Phys.* 12:328–334.

Simons, K., and D. Toomre. 2000. Lipid rafts and signal transduction. *Nat. Rev. Mol. Cell Biol.* 1:31–39.

Stauffer, D., and A. Aharony. 1992. Introduction to Percolation Theory. Taylor and Francis, London, Washington, DC. 17.

Sugar, I. P., and R. L. Biltonen. 2000. Structure-function relationships in two-component phospholipid bilayers. A Monte Carlo simulation approach using a two-state model. *Methods Enzymol.* 323:340–372.

Sugar, I. P., E. I. Michonova-Alexova, and P. L.-G. Chong. 2001. Geometrical properties of gel and fluid clusters in DMPC/DSPC bilayers: Monte Carlo simulation approach using a two-state model. *Biophys. J.* 81:2425–2441.

Sugar, I. P., and G. Monticelli. 1985. Interrelationships between the phase diagrams of the two-component phospholipid bilayers. *Biophys. J.* 48: 283–288.

Sugar, I. P., T. E. Thompson, and R. L. Biltonen. 1999. Monte Carlo simulation of two-component bilayers: DMPC/DSPC mixtures. *Biophys. J.* 76:2099–2110.

Sun, H., and I. P. Sugar. 1997. Acceleration of convergence to the thermodynamic equilibrium by introducing shuffling operations to the Metropolis algorithm of Monte Carlo simulations. *J. Phys. Chem. B.* 101: 3221–3227.

Thompson, T. E., M. B. Shankaram, R. L. Biltonen, D. Marsh, and W. L. C. Vaz. 1995. Effects of domain structure on in-plane reactions and interactions. *Mol. Membr. Biol.* 12:157–162.

Tocanne, J. F. 1992. Detection of lipid domains in biological membranes. *Comm. Mol. Cell. Biophys.* 8:53–72.

Van Dijck, P. W. M., A. J. Karper, H. A. J. Oonk, and J. De Gier. 1977. Miscibility properties of binary phosphatidylcholine mixtures: a calorimetric study. *Biochim. Biophys. Acta.* 470:58–69.

Vaz, W. L. C., E. C. C. Melo, and T. E. Thompson. 1989. Translational diffusion and fluid domain connectivity in a two-component, two-phase phospholipid bilayer. *Biophys. J.* 56:869–876.

Verkade, P., and K. Simons. 1997. Lipid microdomains and membrane trafficking in mammalian cells. *Histochem. Cell. Biol.* 108:211–220.

Von Dreele, P. H. 1978. Estimation of lateral species separation from phase transitions in nonideal two-dimensional lipid mixtures. *Biochemistry.* 17:3939–3943.

Welby, M., Y. Poquet, and J. F. Tocanne. 1996. The spatial distribution of phospholipids and glycolipids in the membrane of the bacterium *Micrococcus Iuteus* varies during the cell cycle. *FEBS. Lett.* 384:107–111.

Welty, R., and M. Glaser. 1994. Lipid domains in model and biological membranes. *Chem. Phys. Lipids.* 73:121–137.

Wilkinson, D. A., and J. F. Nagle. 1979. Dilatometric study of binary mixtures of phosphatidylcholines. *Biochemistry.* 18:4244–4249.

Yang, L., and M. Glaser. 1996. Formation of membrane domains during the activation of protein kinase C. *Biochemistry.* 35:13966–13974.